Enhanced Intersystem Crossing Rate in Polymethine-Like Molecules: Sulfur-Containing Squaraines versus Oxygen-Containing Analogues

ARTICLE *in* THE JOURNAL OF PHYSICAL CHEMISTRY A · FEBRUARY 2013

Impact Factor: 2.69 · DOI: 10.1021/jp400276g · Source: PubMed

THE JOURNAL OF PHYSICAL CHEMISTRY A

Article

pubs.acs.org/JPCA

Enhanced Intersystem Crossing Rate in Polymethine-Like Molecules: Sulfur-Containing Squaraines versus Oxygen-Containing Analogues

Davorin Peceli,[†] Honghua Hu,[†] Dmitry A. Fishman,[†] Scott Webster,[†] Olga V. Przhonska,[†,‡] Vladimir V. Kurdyukov,[§] Yurii L. Slominsky,[§] Alexey I. Tolmachev,[§] Alexey D. Kachkovski,[§] Andrey O. Gerasov,[§] Artëm E. Masunov,[∥,⊥,#,○] David J. Hagan,[†,#] and Eric W. Van Stryland*[,†,#]

[†]CREOL: College of Optics and Photonics, University of Central Florida, Orlando, Florida 32816, United States

[‡]Institute of Physics, National Academy of Sciences, Kiev, 03028, Ukraine

[§]Institute of Organic Chemistry, National Academy of Sciences, Kiev, 03094, Ukraine

[∥]NanoScience Technology Center, University of Central Florida, Orlando, Florida 32826, United States

[⊥]Department of Chemistry, University of Central Florida, Orlando, Florida 32816, United States

[#]Department of Physics, University of Central Florida, Orlando, Florida 32816, United States

[○]Florida Solar Energy Center, University of Central Florida, Cocoa, Florida 32922, United States

ABSTRACT: Two different approaches to increase intersystem crossing rates in polymethine-like molecules are presented: traditional heavy-atom substitution and molecular levels engineering. Linear and nonlinear optical properties of a series of polymethine dyes with Br- and Se-atom substitution, and a series of new squaraine molecules, where one or two oxygen atoms in a squaraine bridge are replaced with sulfur atoms, are investigated. A consequence of the oxygen-to-sulfur substitution in squaraines is the inversion of their lowest-lying $\pi\pi^*$ and $n\pi^*$ states leading to a significant reduction of singlet−triplet energy difference and opening of an additional intersystem channel of relaxation. Experimental studies show that triplet quantum yields for polymethine dyes with heavy-atom substitutions are small (not more than 10%), while for sulfur-containing squaraines these values reach almost unity. Linear spectroscopic characterization includes absorption, fluorescence, quantum yield, anisotropy, and singlet oxygen generation measurements. Nonlinear characterization, performed by picosecond and femtosecond laser systems (pump−probe and Z-scan measurements), includes measurements of the triplet quantum yields, excited state absorption, two-photon absorption, and singlet and triplet state lifetimes. Experimental results are in agreement with density functional theory calculations allowing determination of the energy positions, spin−orbital coupling, and electronic configurations of the lowest electronic transitions.

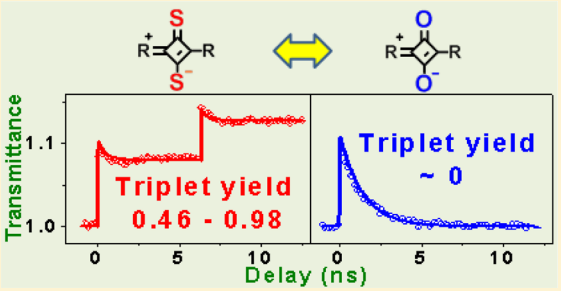

1. INTRODUCTION

Polymethine dyes (PDs) have been known for more than a century and have found numerous applications as photosensitizers in photography and photodynamic therapy, fluorescent probes in chemistry and biology, active and passive laser media, materials for nonlinear optics and electroluminescence, memory devices, etc.[1−4] These compounds exhibit a large molar absorbance (up to 3×10^5 M^{-1}) and tunable absorption bands in the visible and near-infrared regions important for the development of organic materials with large nonlinearities for nonlinear optical applications. On the basis of the number of methine (—CH═) groups in the π-conjugation, linear conjugated compounds can be formally divided into *polymethines* (containing an *odd number* of methine groups with alternating single and double bonds) and *polyenes* (containing an *even number* of methine groups). As commonly accepted, these two families of dyes have distinctive electronic structures, and thus differ by their linear and nonlinear optical properties.[5−7] The electronic properties of PDs can be tailored by changing the length of the conjugation chain and by adding specific electron acceptor (A) or electron donor (D) terminal groups, thus forming the following molecular structures: cationic D-π-D, anionic A-π-A, and neutral D-π-A. Additionally, electron acceptor or donor groups may be included in the main π-conjugation chain, resulting in the neutral quadrupolar structures, such as D-π-A-π-D or A-π-D-π-A. Squaraine (or squarylium) dyes (SDs), which are the main subject of the current work, may be considered as compounds from the polymethine family, as they combine polymethine (odd) number of carbon atoms in the chain with an electron acceptor C_4O_2 bridge at the center of the conjugated chromophore. PDs are extensively studied, and many of their linear and nonlinear

Received: January 9, 2013
Revised: February 19, 2013
Published: February 21, 2013

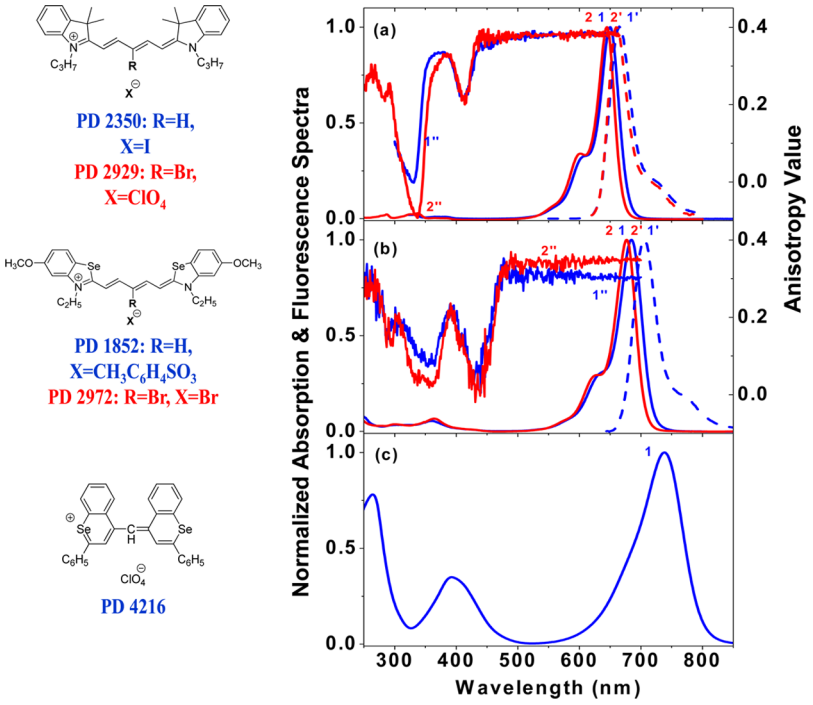

Figure 1. Molecular structures, absorption (solid lines 1, 2), fluorescence (dashed lines 1′, 2′), and anisotropy (1″, 2″) for (a) PD 2350 (1, 1′, and 1″) and PD 2929 (2, 2′, and 2″); (b) PD 1852 (1, 1′, and 1″) and PD 2972 (2, 2′, and 2″); (c) PD 4216 in ACN (1). Absorption and fluorescence spectra are measured in ethanol; anisotropy spectra are measured in glycerol. No fluorescence was detected for PD 4216.

properties are well-understood.[8−11] Structure−property relations are developed allowing one not only to predict the main properties of existing compounds but also to synthesize new ones with desirable optical properties. The missing link in this study for PD-like molecules is the clear understanding of singlet−triplet (S−T) conversion processes, which are usually characterized by small triplet quantum yields (Φ_T), ~10^{-2}−10^{-4}.[12−14] Typically, with nano-, pico-, or femtosecond pulse durations, the population of the triplet states is negligibly small and only singlet−singlet (S−S) transitions are needed for the analysis of linear and nonlinear processes.

To our knowledge, the nature of the vanishingly small intersystem crossing rate, k_{ST}, in polymethine-like molecules has not been systematically interpreted in the literature, and the strategy to design PDs with an increased probability of triplet formation has not been proposed. In our recent paper,[15] we described an approach to design PD-like molecules with simultaneously large Φ_T, large 2PA cross sections (δ_{2PA}), and large quantum yield of singlet oxygen generation (Φ_Δ). These compounds can be potentially useful for application in two-photon photodynamic therapy[14,16−18] and optical power limiting requiring strong S−S and triplet−triplet (T−T) excited state absorption.[19−22]

In the current paper, we provide some insights into the nature of intersystem crossing (ISC) processes in polymethine-like molecules and discuss the methods of k_{ST} enhancement. It is well-known that k_{ST} can be approximated by Fermi's golden rule for radiationless transitions as[23,24]

$$k_{ST} = \frac{2\pi}{\hbar}\rho\langle\psi(S)|H_{SOC}|\psi(T)\rangle^2 \quad (1)$$

where $\langle\psi(S)|H_{SOC}|\psi(T)\rangle$ is the spin−orbit coupling (SOC) matrix element with corresponding SOC Hamiltonian, H_{SOC}, and ρ is the Franck−Condon weighted density of states representing energy conservation, and thus, depending on the singlet−triplet splitting energy, ΔE, H_{SOC} can be written as[25,26]

$$H_{SOC} = \alpha^2 \sum_{\mu}^{N} \sum_{i}^{n} \frac{Z_\mu}{r_{i\mu}^3} L_i S_i \quad (2)$$

where α is the fine-structure constant, Z is the effective charge on nucleus μ, $r_{i\mu}$ is the distance between the ith electron and μth nucleus, and S_i and L_i are the spin and orbital angular moments of the ith electron, respectively. The summation runs over all electrons (n) and nuclei (N). The Franck−Condon density of states ρ at room temperature (T) can be evaluated in the form of a Boltzmann distributed population as[27]

$$\rho = \frac{1}{\sqrt{4\pi\lambda_M RT}} \exp\left[-\frac{(\Delta E_{ST} + \lambda_M)^2}{4\lambda_M k_B T}\right] \quad (3)$$

where λ_M is the so-called Marcus reorganization energy which includes both intramolecular and solvent-induced relaxations, k_B is the Boltzmann constant, and ΔE_{ST} is the singlet−triplet splitting energy. As seen from eqs 1−3, two main parameters contribute to the intersystem crossing rate k_{ST}: the spin−orbit coupling Hamiltonian H_{SOC}, which is sensitive to the effective nuclear charge Z, and singlet−triplet splitting energy ΔE_{ST}.

The traditional method to increase the SOC is the introduction of atoms with large atomic numbers to the molecular structure. According to eq 2, H_{SOC} is proportional to Z/r^3, and an increase of Z leads to a higher rate of ISC. This effect is well-known as the "heavy-atom" effect.[25,26,28]

The new method introduced in our previous paper[15] for squaraine dyes is based on specific molecular level engineering, leading to a decrease of the singlet−triplet energy difference. We showed that the replacement of two oxygen atoms in a squaraine bridge with two sulfur atoms leads to an inversion of the lowest singlet π,π^* excited state with respect to the n,π^*

dx.doi.org/10.1021/jp400276g | J. Phys. Chem. A 2013, 117, 2333−2346

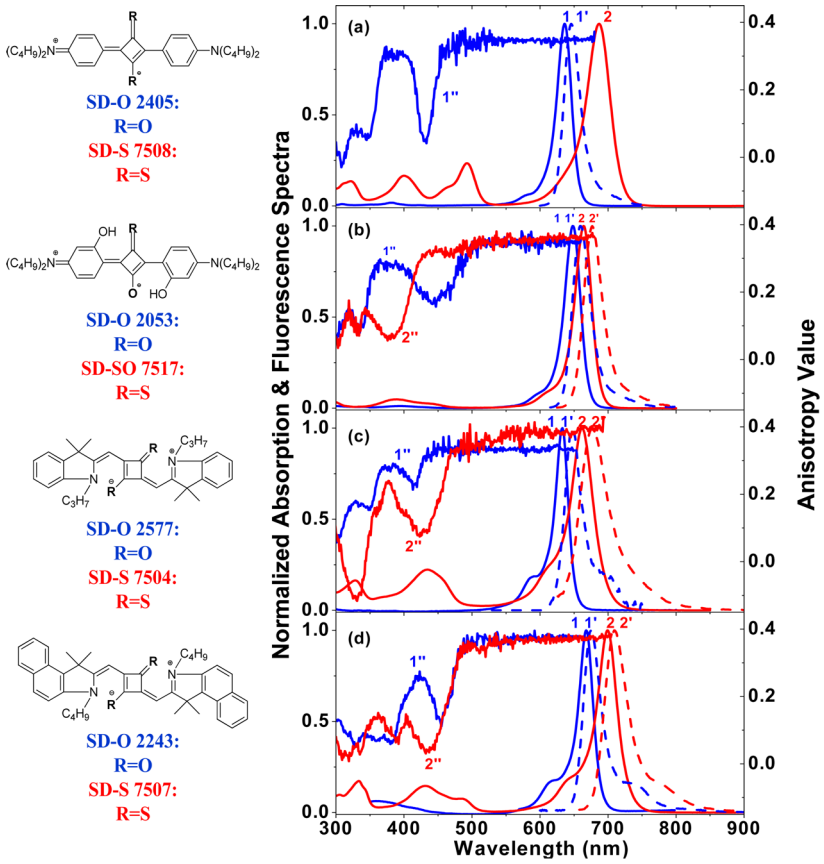

Figure 2. Molecular structures, absorption (solid lines 1, 2), fluorescence (dashed lines 1′, 2′), and anisotropy (1″, 2″) for (a) SD−O 2405 (1, 1′, and 1″) and SD−S 7508 (1) in toluene; (b) SD−O 2053 (1, 1′, and 1″) and SD−SO 7517 (2, 2′, and 2″) in DCM; (c) SD−O 2577 (1, 1′, and 1″) in ethanol and SD−S 7504 (2, 2′, and 2″) in toluene; (d) SD−O 2243 (1, 1′, and 1″) in DCM and SD−S 7507 (2, 2′, and 2″) in toluene. All anisotropy spectra are measured in pTHF. No fluorescence was detected for SD−S 7508.

excited state. This inversion significantly enhances H_{SOC} in three ways. First, this inversion creates the possibility of effective mixing of the singlet and triplet states of different molecular orbital configurations (El-Sayed rule[29]), thus increasing spin−orbit coupling efficiency. Second, the inversion leads to a significant decrease of ΔE_{ST}.[30] Third, the dark n,π^* singlet excited state has a much longer radiative lifetime, allowing the radiationless ISC channel to dominate.

In the current paper, we perform a thorough investigation of the linear and nonlinear optical properties of a series of PDs with Br- and Se-atom substitution and a series of new SDs, where one or two oxygen atoms in a squaraine bridge are replaced with sulfur atoms. Studies of linear spectroscopic properties include absorption, fluorescence, quantum yield, and anisotropy measurements, as well as determination of singlet oxygen generation quantum yields. Nonlinear properties, determined with pico- and femtosecond laser systems by single and double pump probe[31,32] and *Z*-scan techniques,[33] include determination of ISC quantum yields (i.e., triplet quantum yields), singlet−singlet and triplet−triplet excited state absorption, two-photon absorption, and singlet and triplet state lifetimes. We show that the heavy-atom effect does not significantly enhance ISC in PDs: they are still characterized by small triplet quantum yields (≤10%), while the values of ISC and singlet oxygen generation quantum yields for sulfur-containing SDs reach almost unity. We perform a detailed comparison of a series of sulfur-containing squaraines versus their oxygen-containing analogues and show that sulfur substitution in SDs significantly affects the ISC rate while making almost no change to their nonlinear optical properties such as two-photon and excited state absorption. Experimental results are in agreement with quantum chemical calculations, allowing the determination of the energy levels and the leading molecular orbital configurations responsible for the lowest singlet and triplet electronic transitions.

2. EXPERIMENTAL METHODS AND RESULTS

2.1. Materials Characterization and Linear Spectroscopic Properties. The molecular structures of the dyes studied in this paper are shown in Figures 1 and 2. They are separated into two groups. The first group (Figure 1) reflects our attempts to enhance k_{ST} in PDs due to the heavy-atom effect by designing molecules with the heavy-atom substitutions. These molecules contain a Br atom connected to the π-conjugated chain (labeled as PD 2929) in comparison with the analogous unsubstituted PD 2350, Se atoms incorporated into the terminal groups (labeled as PD 1852 and PD 4216), and both Se-substituted terminal groups and a Br-atom substitution within the π-conjugated chain (labeled as PD 2972). The second group of compounds (Figure 2) correspond to the introduction of atoms with unshared pairs of electrons producing n → π^* transitions. They are squaraines with oxygen (labeled as SD−O) and with sulfur (labeled as SD−S/SD−SO) atoms in the central acceptor C_4O_2 (or C_4S_2/C_4SO) fragments. All eight SDs are paired as SD−O 2405 and SD−S 7508, SD−O 2577 and SD−S 7504, SD−O 2243 and SD−S

dx.doi.org/10.1021/jp400276g | J. Phys. Chem. A 2013, 117, 2333−2346

Table 1. Photophysical Parameters[a]

dye (solvent)	λ_{Abs}^{max} (nm)	λ_{FL}^{max} (nm)	ε^{max} ($\times 10^5$ M^{-1} cm^{-1})	Φ_F	τ_s calculated (ns)	τ_S experiment (ns)	Φ_T	Φ_Δ	τ_{T10} (air saturated solvent) (μs)	τ_{T10} (nitrogen purged solvent) (μs)
PD 2350 (EtOH)	646	665	2.36	0.32 ± 0.03	0.98	0.95 ± 0.03	0			
PD 2929[b] (EtOH)	645	660	2.67	0.10 ± 0.01	0.27	0.30 ± 0.03	0.05 ± 0.05	nondetectable		
PD 1852[b] (EtOH)	685	706	2.05	0.33 ± 0.03	1.3	1.0 ± 0.1	0.10 ± 0.05	nondetectable	0.29 ± 0.03	
PD 2972[b] (EtOH)	677	692	2.28	0.16 ± 0.02	0.55	0.50 ± 0.04	0.09 ± 0.05	nondetectable	0.07 ± 0.01	
PD 4216 (ACN)	738	nondetectable	0.42	<0.001		0.8 ± 0.3 (ps)	0			
SD−O 2405[b] (TOL)	636	646	3.64	1.0 ± 0.1	2.3	2.2 ± 0.2	0			
SD−S 7508[b] (TOL)	687	nondetectable	1.57	<0.001		4.5 ± 0.5 (ps)	0.98 ± 0.02	1.0 ± 0.2	0.24 ± 0.04	0.6 ± 0.1 and 3.4 ± 0.3
SD−O 2577 (DCM)	636	642	3.57	0.27 ± 0.03	0.7	0.9 ± 0.1	0			
SD−S 7504 (TOL)	678	691	1.59	0.12 ± 0.01	0.5	0.50 ± 0.05	0.75 ± 0.03	0.50 ± 0.01	0.30 ± 0.05	0.4 ± 0.04 and 1.9 ± 0.2
SD−O 2243 (DCM)	668	675	3.45	0.36 ± 0.04	1.0	1.3 ± 0.1	0			
SD−S 7507 (TOL)	697	709	1.92	0.25 ± 0.03	1	1.5 ± 0.2	0.46 ± 0.04	0.20 ± 0.05	0.29 ± 0.05	0.6 ± 0.1 and 2.9 ± 0.3
SD−O 2053 (DCM)	648	660	4.23	0.95 ± 0.05	2.1	2.3 ± 0.4	0			
SD−SO 7517 (ACN)	661	669	3.16	0.28 ± 0.03	1.1	1.4 ± 0.2	0.64 ± 0.03	0.70 ± 0.2	0.30 ± 0.05 (TOL)	1.0 ± 0.1 and 4.4 ± 0.4 (TOL)
									0.20 ± 0.05 (ACN)	0.6 ± 0.1 (ACN)

[a] λ_{Abs}^{max} and λ_{Fl}^{max} are the peak absorption and fluorescence wavelengths; ε^{max} is the peak extinction coefficient; Φ_F is the fluorescence quantum yield; τ_S is the lifetime of the lowest singlet excited state; Φ_T and Φ_Δ are the triplet and singlet oxygen generation quantum yields, respectively; and τ_{T10} is the lifetime of the lowest triplet excited state. Two components in τ_{T10} (last column) correspond to double exponential decays observed in toluene. Solvent abbreviations: ethanol (EtOH), toluene (TOL), acetonitrile (ACN), and dichloromethane (DCM). [b] A portion of the data was previously published in letter format, see ref 15.

dx.doi.org/10.1021/jp400276g | J. Phys. Chem. A 2013, 117, 2333−2346

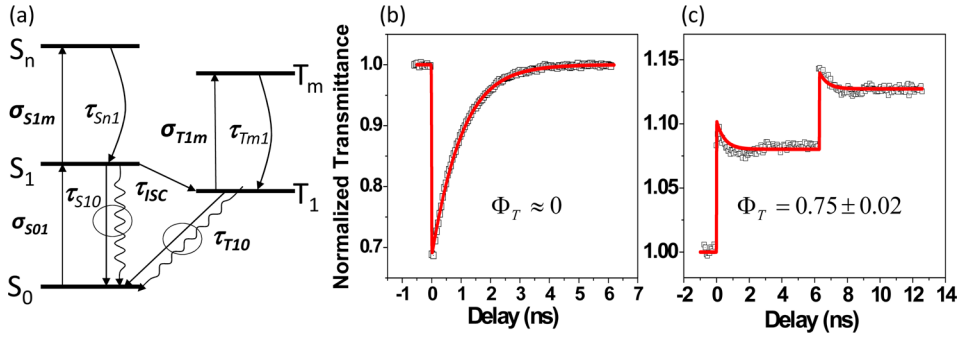

Figure 3. (a) Five-level energy diagram (see description in the text); (b) single pump−probe measurements for SD−O 2577 in DCM at 532 nm (linear transmittance 0.7, pump fluence 3.8 mJ/cm^2, $\sigma_{S01} = 8.8 \times 10^{-18}$ cm^2, $\sigma_{S1n} = 1.3 \times 10^{-16}$ cm^2, $\tau_S = 0.9$ ns); (c) DPP measurements for SD−S 7504 in toluene at 670 nm (linear transmittance 0.75, fluence in each pump 0.33 mJ/cm^2, $\sigma_{S01} = 5.2 \times 10^{-16}$ cm^2, $\sigma_{S1n} = (2.6 \pm 0.5) \times 10^{-16}$ cm^2, $\sigma_{T1n} = (2.5 \pm 0.5) \times 10^{-16}$ cm^2, $\tau_S = 0.50 \pm 0.05$ ns).

7507, and SD−O 2053 and SD−SO 7517 (containing one sulfur and one oxygen). Each pair of dyes contains the same donor terminal groups and identical polymethine chain length and differs only by oxygen or sulfur substitution in the central acceptor fragment.

The linear absorption spectra of all molecules, recorded by a Varian Cary 500 spectrophotometer, are presented in Figures 1 and 2. The choice of solvents is based on the solubility of the dyes and includes ethanol (EtOH), toluene (TOL), acetonitrile (ACN), and dichloromethane (DCM). The absorption spectra for all dyes are composed of intense cyanine-like bands attributed to their $\pi\pi^*$ $S_0 \rightarrow S_1$ transitions, and weaker higher-lying $S_0 \rightarrow S_n$ transitions in the visible and ultraviolet regions. The absorption spectra of PDs with and without Br substitution, shown in Figure 1, are similar, reflecting that a Br atom placed in the meso-position of the π-conjugated chain does not significantly affect the charge distribution within the chain. The absorption spectrum of PD 4216 is strongly red-shifted even for this short chain length and shows a relatively intense absorption around 400 nm due to the existence of own π-conjugation system in the terminal groups decreasing the HOMO/LUMO gap. The main absorption bands for all SD−S dyes, shown in Figure 2, are red-shifted (≈30−50 nm) in comparison to their SD−O analogues, and their higher-lying transitions are more intense, which can be explained by the existence of a π-conjugation system in the perpendicular S−S chromophore. Note that for SD−SO 7517, of which only one oxygen atom is replaced by a sulfur atom, the red-shift of the main absorption band is significantly less, ∼13 nm with respect to its counterpart SD−O 2053. All SD−S dyes are less photochemically stable than SD−O dyes, which require special care in experimental studies.

The fluorescence spectra of all compounds, corrected for the spectral responsivity of the detection system, are measured by a PTI QuantaMaster spectrofluorimeter and shown in Figures 1 and 2. We note the spectral mirror symmetry between absorption and fluorescence spectra for all compounds reflecting only a small change in the excited state geometry upon excitation. Fluorescence quantum yields, Φ_F, are measured using the standard method of comparison with a known reference dye, Cresyl Violet perchlorate (CAS# 41830-80-2, Sigma Aldrich) in methanol, which has an absorption peak at 594 nm, fluorescence peak at 620 nm, and a fluorescence quantum yield, $\Phi_F = 0.54 \pm 0.03$.[34] No fluorescence ($\Phi_F < 0.001$) is observed for SD−S 7508 and PD 4216, however, for different reasons. As to be shown in section 2.2, SD−S 7508 is characterized by near unity triplet quantum yield (Φ_T), indicating the ISC process as the most effective channel for nonradiative decay of the S_1 state, while the main radiationless path for PD 4216 is internal conversion due to its strongly nonplanar structure.

From spectroscopic measurements, we estimate the fluorescence lifetime, $\tau_F = \Phi_F \tau_N$, where the natural lifetime, τ_N, can be calculated from the Strickler−Berg equation:[35]

$$\frac{1}{\tau_N} = 2.88 \times 10^{-9} n^2 \varepsilon^{\max} \frac{\int F(\nu)\, d\nu \times \int \frac{\varepsilon(\nu)}{\nu}\, d\nu}{\int \frac{F(\nu)}{\nu^3}\, d\nu} \quad (4)$$

where $F(\nu)$ and $\varepsilon(\nu)$ are the normalized fluorescence and absorption spectra in wavenumber (ν, cm^{-1}), ε^{max} is the molar absorbance at the peak of the absorption band (M^{-1} cm^{-1}), and n is the refractive index of the solvent. For all compounds, eq 4 gives reasonably good agreement (within ∼20%, see Table 1) of the fluorescence lifetimes calculated and directly measured by a pico- and femtosecond pump−probe technique (see section 2.2).

Excitation anisotropy measurements allow determining the spectral positions of the optical transitions and relative orientation of the transition dipole moments.[35] These measurements are performed using viscous solutions of glycerol or poly tetrahydrofuran (pTHF) to reduce rotational reorientation and at low concentrations ($C \approx 1$ μM) to avoid reabsorption of the fluorescence. The anisotropy value r for a given excitation wavelength λ can be calculated as $r(\lambda) = [I_{\parallel}(\lambda) - I_{\perp}(\lambda)]/[I_{\parallel}(\lambda) + 2I_{\perp}(\lambda)]$, where $I_{\parallel}(\lambda)$ and $I_{\perp}(\lambda)$ are the intensities of the fluorescence signal (typically measured near the fluorescence maximum) polarized parallel and perpendicular to the excitation light, respectively. Excitation anisotropy spectra, shown in Figures 1 and 2, reveal alternating peaks and valleys. The peaks in the excitation anisotropy spectrum indicate a small angle between the absorption and emission transition dipoles, suggesting allowed one-photon absorption (1PA) transitions, while valleys indicate large angles between these two dipoles, suggesting forbidden 1PA transitions, such as transitions between states of the same symmetry. Due to selection rules for symmetrical cyanine-like dyes, these valleys in the anisotropy spectra could indicate the positions of allowed 2PA transitions. Thus, as was shown by us previously, excitation anisotropy spectra can serve as a useful guide to predict the positions of the final states in the 2PA spectra of cyanine-like dyes.[36]

dx.doi.org/10.1021/jp400276g | J. Phys. Chem. A 2013, 117, 2333−2346

The direct measurements of singlet oxygen, $^1O_2$, luminescence at ~1270 nm were performed at room temperature using a PTI QuantaMaster spectrofluorometer with a nitrogen cooled Hamamatsu R5509-73 photomultiplier tube detector. $^1O_2$ generation quantum yields (Φ_Δ) were measured in comparison with the known dye acridine in ACN with $\Phi_\Delta = 0.82$[37] at room temperature with air-saturated solution.

The most significant linear properties for the dyes studied are listed in Table 1.

2.2. Nonlinear Characterization Methods and Results. Nonlinear optical investigations include a broad range of femto- and picosecond pulsewidth measurements with the goal of determining the ISC transition rates, formation of the excited state singlet−singlet (S−S) and triplet−triplet (T−T) absorption bands, singlet and triplet state lifetime dynamics, and precisely determine the important molecular parameters such as triplet (Φ_T) and singlet oxygen generation (Φ_Δ) quantum yields.

The picosecond system used is a 10 Hz Nd:YAG laser (EKSPLA PL2143) pumping an optical parametric generator/amplifier (OPG/A) (PG401/DFG) tunable from 0.42 to 2.3 μm with a pulsewidth of 25 ps (fwhm) measured with a second-harmonic autocorrelation technique. The femtosecond system is composed by a Ti:sapphire regenerative amplifier (Clark-MXR, CPA 2011, delivering 1.6 mJ pulses at 780 nm, with a 1 kHz repetition rate and a pulsewidth of ~150 fs, fwhm), pumping two OPG/OPAs (Light Conversion Ltd., model TOPAS-800). The wavelength tuning range is from 0.3 to 2.6 μm.

2.2.1. Single and Double Pump−Probe Techniques. Decay kinetics and population dynamics of organic molecules are usually described with the standard five-level energy diagram, shown in Figure 3a. It is well-known that there are several competing processes to depopulate the S_1 state which include: (1) radiative (fluorescence) and nonradiative (internal conversion) decays into the singlet ground state S_0 with lifetime τ_{S10}; (2) excitation to the higher-lying singlet states S_n by sequential absorption of another photon (S_1−S_n absorption); (3) ISC leading to population of a triplet state T_1 with lifetime τ_{ISC}. Note that the lifetime of the T_1 state is long (usually 10^{-6}−10^2 s)[38−40] due to the spin-forbidden nature of a triplet−singlet transition; (4) excitation to the higher-lying triplet states T_m by sequential absorption of another photon (T_1−T_m absorption); and (5) radiative (phosphorescence) or nonradiative decays from T_1 into S_0. The singlet lifetime including radiative and nonradiative decays, τ_S, can be written as $1/\tau_S = 1/\tau_{S10} + 1/\tau_{ISC}$.

To mathematically describe the physical processes shown in Figure 3a, the propagation (5) and rate (6) equations can be employed:[41]

$$\frac{dI}{dz} = -\sigma_{S01}N_{S0}I - \sigma_{S1n}N_{S1}I - \sigma_{T1m}N_{T1}I \quad (5)$$

$$\frac{dN_{S0}}{dt} = -\frac{\sigma_{S01}N_{S0}I}{\hbar\omega} + \frac{N_{S1}}{\tau_{S10}} + \frac{N_{T1}}{\tau_{T10}}$$

$$\frac{dN_{S1}}{dt} = \frac{\sigma_{S01}N_{S0}I}{\hbar\omega} - \frac{N_{S1}}{\tau_{S10}} - \frac{\sigma_{S1n}N_{S1}I}{\hbar\omega} + \frac{N_{Sn}}{\tau_{Sn1}} - \frac{N_{S1}}{\tau_{ISC}}$$

$$\frac{dN_{Sn}}{dt} = \frac{\sigma_{S1n}N_{S1}I}{\hbar\omega} - \frac{N_{Sn}}{\tau_{Sn1}}$$

$$\frac{dN_{T1}}{dt} = -\frac{\sigma_{T1m}N_{T1}I}{\hbar\omega} + \frac{N_{Tm}}{\tau_{Tm1}} + \frac{N_{S1}}{\tau_{ISC}} - \frac{N_{T1}}{\tau_{T10}}$$

$$\frac{dN_{Tm}}{dt} = \frac{\sigma_{T1m}N_{T1}I}{\hbar\omega} - \frac{N_{Tm}}{\tau_{Tm1}} \quad (6)$$

where I is the irradiance; z is the depth in the sample; σ_{ij} and τ_{ij} are cross sections and lifetimes relating to the particular singlet and triplet transitions, respectively; τ_S and τ_{T10} are the singlet and triplet lifetimes, both including radiative and nonradiative decays; N_{S0}, N_{S1}, N_{Sn}, N_{T1}, and N_{Tm} are populations of the singlet (S_0, S_1, and S_n) and triplet (T_1 and T_m) states, respectively. The total population, $N = N_{S0} + N_{S1} + N_{Sn} + N_{T1} + N_{Tm}$, is conserved. Since the lifetimes τ_{Sn1} and τ_{Tm1} are usually short (sub-picosecond), the populations of the higher-lying singlet (N_{Sn}) and triplet (N_{Tm}) states can be neglected in the analysis. The triplet quantum yield (Φ_T), as a fraction of the population moved to the triplet state, can be defined as

$$\Phi_T = \frac{\tau_S}{\tau_{ISC}} = \frac{\tau_{S10}}{\tau_{S10} + \tau_{ISC}} = \frac{k_{ISC}}{k_F + k_{ISC}} \quad (7)$$

The pump−probe technique is the most common technique for time-resolved studies.[42,43] A strong laser pulse (pump) is used to change the population and optical properties of the sample and a much weaker pulse (probe, with irradiance usually less than 5% of the pump irradiance to prevent any nonlinear effects from the probe beam) is used to study the magnitude and time evolution of the induced changes. The probe spot size at the sample is typically set ~10× smaller than the pump size, and the angle between pump and probe is typically small, ~5°, to ensure that the probe beam travels through the homogeneously pumped solution. The polarization angle between the pump and probe is set to the magic angle (54.7°) to avoid contributions from orientational effects.[44] The magnitude of nonlinear optical changes, for example, the excited state absorption (ESA) cross sections, can be determined by solving eqs 5−6, for known pump beam waist and pulse energy. The time evolution is investigated by delaying the probe pulse with respect to the pump and by monitoring the probe transmittance with various time delays. The temporal accuracy of the measurements is defined mainly by the pump pulsewidth. Since the singlet state lifetimes of almost all molecules in this work range from 500 ps to 1.5 ns, most pump−probe measurements are done with the picosecond laser system. The only exceptions are PD 4216 and SD−S 7508, whose short lifetimes of ~1 and 4.5 ps, respectively, were determined with the femtosecond laser system. In both pico- and femtosecond setups, the spot sizes (HW/e^2 M) of the pump and probe beams were measured by knife-edge scans and equal to ~200 and ~20 μm, respectively.

For the molecules with small ISC (for example, SD−O molecules), the populations of the triplet states are negligible, and the five-level model can be reduced to a three-level model

accounting for the singlet states only. An example of the experimental decay kinetics and its numerical simulation for SD−O 2577 is shown in Figure 3b. The measurement was done at pump and probe wavelengths of 532 nm in the reverse saturable absorption (RSA) region where $\sigma_{S1n} \gg \sigma_{S01}$. Pump−probe dynamics show a complete recovery of the initial transmittance after a few nanoseconds time delay, indicating a negligible population of the triplet state. By fitting experimental pump−probe dynamics using simplified eqs 5 and 6, the values of σ_{S1n} and τ_S are determined as $\sigma_{S1n} = 1.3 \times 10^{-16}$ cm^2 and τ_S = 0.9 ns. However, for some molecules, ISC can be significant (for example, for SD−S molecules), and a significant fraction of initial ground state population can be redistributed to the triplet state. Therefore, the five-level model cannot be simplified. In this case, a classical single pump−probe method cannot simultaneously determine the singlet and triplet state absorption parameters and transition rates. The double pump−probe (DPP) technique, first introduced by Swatton et al.,[31] is a variant of the standard pump−probe scheme but uses two strong pumps instead of one to create two sets of initial conditions for solving eqs 5 and 6. This method allows for a unique determination of Φ_T, not requiring the use of a reference sample, with simultaneous determination of σ_{T1m} in the same experiment. Two strong pump pulses, usually (but not necessarily) having the same wavelengths and pulse energies, are separated by a time delay chosen to allow for significant depopulation of the singlet excited states via decay to S_0 and via ISC to the triplet state. The second pump interacts with the modified molecular system, and the initial conditions for solving the rate equations are different. Numerical fitting of eqs 5 and 6 after both the first and second pumps allows for a unique determination of Φ_T and σ_{T1m}. For most molecules, the picosecond DPP technique can be used; however, for the molecules with ultrafast ISC rates,[45−47] femtosecond pumps may be required.[32] A detailed description of the DPP technique and methods for its optimization are described in our paper.[32] An example of the experimental DPP decay kinetics and its numerical simulation for SD−S 7504 are shown in Figure 3c. This measurement was done at a pump and probe wavelength of 670 nm in the saturable absorption (SA) region, close to the peak of linear absorption where $\sigma_{S1n} \ll \sigma_{S01}$. The large value of σ_{S01} ensures that a large fraction of ground state population is moved to the triplet state which significantly improves the accuracy for determining the triplet quantum yield. By fitting the DPP dynamics, the values of σ_{S1n}, σ_{T1m}, Φ_T, and τ_S are determined as $\sigma_{S1n} = (2.6 \pm 0.5) \times 10^{-16}$ cm^2, $\sigma_{T1m} = (2.5 \pm 0.5) \times 10^{-16}$ cm^2, $\Phi_T = 0.75 \pm 0.03$, and $\tau_S = 0.50 \pm 0.05$ ns.

Note that all triplet yield measurements were performed in air-saturated solutions. We also checked the effect of oxygen on Φ_T and τ_S by partially removing the oxygen owing to bubbling solutions with nitrogen gas stream for about half an hour. We found that removing the oxygen from the samples does not significantly affect Φ_T and τ_S values. Note that we did not attempt to measure the oxygen concentration before and after bubbling; however, the oxygen concentration after bubbling was decreased significantly, thus affecting the triplet state lifetimes (see section 2.2.3). The main results of single and DPP measurements are given in Table 1.

As seen from Table 1, the largest triplet quantum yields are found for sulfur-containing squaraines, from $\Phi_T = 0.46 \pm 0.04$ for SD−S 7507 to $\Phi_T = 0.98 \pm 0.02$ for SD−S 7508, and the smallest measurable triplet yield, $\Phi_T = 0.05 \pm 0.05$, was found for PD 2929 with Br-substitution in the polymethine chain. PD 2350, without heavy atoms in the chemical structure, and PD 4216, with Se atoms incorporated into the terminal groups (due to nonplanar dye structure leading to extremely small τ_S = 1 ps), show negligible ISC, and therefore $\Phi_T \approx 0$. The same negligible ISC was observed for all oxygen-containing squaraines SD−O 2405, SD−O 2577, SD−O 2243, and SD−O 2053.

2.2.2. ESA Measurements. The ESA spectra from S_1 (corresponding to singlet−singlet (S−S) ESA) and T_1 (triplet−triplet (T−T) ESA) states were measured using a femtosecond white light continuum (WLC) pump−probe as described in refs 8, 48, and 49. The pump pulse, generated by an OPG/OPA, was set at a wavelength close to the linear absorption peak of each investigated dye, while the probe pulse, a broadband WLC, is generated by focusing a small portion of fundamental laser pulse (780 nm) onto a 1 cm water cell. In order to improve the signal-to-noise ratio and avoid stimulated emission,[48] the narrow band interference spectral filters (∼10 nm bandwidth) were used to select the probe wavelengths from the WLC spectrum. Several filters with different central wavelengths were used to obtain the complete ESA spectrum. The pump beam was modulated with a mechanical chopper (283 Hz) synchronized with the 1 kHz repetition rate of the fundamental laser. Transmittance of the probe signal was recorded using a lock-in amplifier. For each probe wavelength, λ, the ESA cross section, $\sigma_{S,T1n}(\lambda)$, can be calculated using eq 8:

$$\sigma_{S,T1n} = \sigma_{S01} - (\sigma_{S01}(\lambda_{ESA}) - \sigma_{S,T1n}(\lambda_{ESA})) \times \frac{\ln\left(\frac{T_{NL}}{T_L}\Big|_{\lambda}\right)}{\ln\left(\frac{T_{NL}}{T_L}\Big|_{\lambda_{ESA}}\right)} \quad (8)$$

where σ_{S01} is the ground state absorption cross section measured by spectrophotometer; T_L is the linear transmittance of the probe before the pump beam arrives at the sample; T_{NL} is the transmittance of the probe in the presence of the pump after a fixed delay (i.e., ∼0.5 ps for S−S ESA and ∼25 ns for T−T ESA); and λ_{ESA} is the wavelength where $\sigma_{S,T1n}$ is measured independently by femto/picosecond *Z*-scan or pump−probe techniques.

Figure 4a,c,e shows the ESA spectra for three squaraine molecules SD−O 2053, SD−SO 7517, and SD−O 2045, while Figure 4b,d,f presents their decay kinetics measured by degenerate picosecond pump−probe with wavelength set to the RSA region. Oxygen-substituted SDs (i.e., SD−O 2053 and SD−O 2405) show only S−S ESA, and their decay kinetics demonstrate a complete restoration of the ground state population within several nanoseconds (Figure 4b,f). In contrast, the decay kinetics of the oxygen−sulfur-substituted SD−SO 7517 shows a nonrecovery of the ground state population beyond 4 ns (Figure 4d), indicating a significant population built up in the long-lived triplet state. Figure 4d shows that σ_{S1n} and σ_{T1n} values for SD−SO 7517 at the peaks of S−S and T−T ESA spectra are comparable. The similarity of S−S ESA in two dyes, SD−O 2053 and its analogue SD−SO 7517, is evidence of the insignificant effect of sulfur substitution on the singlet electronic level structure.

Figure 5a represents S−S and T−T ESA spectra for SD−S 7508 ($\Phi_T = 0.98$, $\tau_{ISC} = 4.5$ ps) in toluene, with two distinctive decay kinetics (Figure 5b), measured by femtosecond WLC pump−probe with pump excitation wavelength at 687 nm (i.e., in the linear absorption peak), and two probe wavelengths at

dx.doi.org/10.1021/jp400276g | J. Phys. Chem. A 2013, 117, 2333−2346

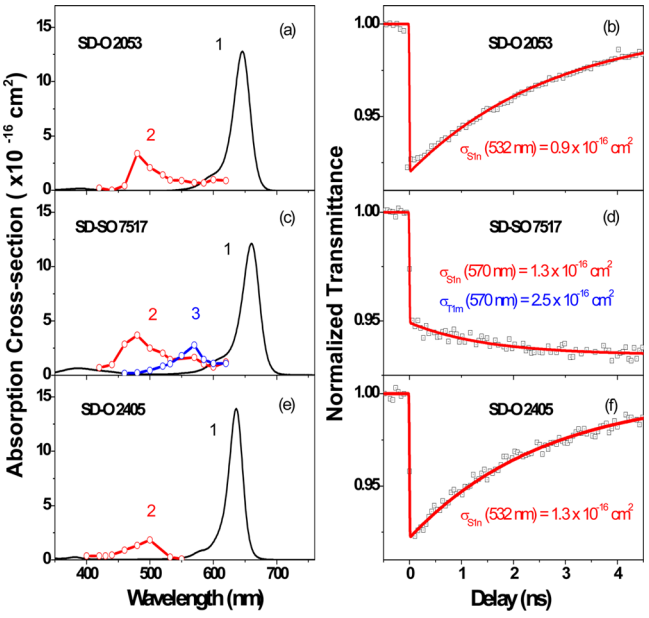

Figure 4. Linear absorption (1), S−S (2), and T−T (3) ESA absorption spectra for (a) SD−O 2053, (b) SD−SO 7517, and (c) SD−O 2405. Decay kinetics for (d) SD−O 2053 at 532 nm (pump fluence 2.6 mJ/cm^2, $\sigma_{S01} = 33 \times 10^{-18}$ cm^2, $\sigma_{S1n} = 0.9 \times 10^{-16}$ cm^2, τ_S = 2.5 ns), (e) SD−SO 7517 at 570 nm (pump fluence 0.5 mJ/cm^2, $\sigma_{S01} = 23 \times 10^{-18}$ cm^2, $\sigma_{S1n} = 1.3 \times 10^{-16}$ cm^2, $\sigma_{T1n} = 2.5 \times 10^{-16}$ cm^2, τ_S = 1.5 ns), and (f) SD−O 2405 at 532 nm (pump fluence 1 mJ/cm^2, $\sigma_{S01} = 9.2 \times 10^{-18}$ cm^2, $\sigma_{S1n} = 1.3 \times 10^{-16}$ cm^2, τ_S = 2.2 ns). SD−O 2053 and SD−SO 7517 are measured in ACN, and SD−O 2405 is measured in toluene.

480 and 570 nm. The probe kinetics at 480 nm (trace 1 in Figure 5b) first shows the RSA process (here $\sigma_{S1n} > \sigma_{S01}$) with a fast decay time of ∼4.5 ps, connected with the rapid depopulation of the S_1 state due to ISC to the T_1 state. Population of the T_1 state leads to T−T ESA with a much slower decay time (>500 ns, as discussed in section 2.2.3), resulting in the SA process (here $\sigma_{T1n} < \sigma_{S01}$). In contrast, the probe dynamics at 570 nm (trace 2 in Figure 5b) shows only RSA. Since σ_{S1n} (570 nm) ≈ σ_{S01} (570 nm), as shown in Figure 5a, the transmittance change connected with S−S ESA is not observable, and the probe kinetics reflects the T−T ESA process only (where $\sigma_{T1n} > \sigma_{S01}$) with a much longer lifetime.

2.2.3. Triplet State Lifetime Measurements. Triplet state lifetimes, τ_{T10}, at room temperature were measured with a modified picosecond pump−probe setup, where the pump beam was set at a wavelength close to the linear absorption peak of each investigated dye, and a CW, frequency doubled Nd:YAG laser at 532 nm was used as the probe beam. The transmittance of the sample was recorded by a digital oscilloscope, Tektronix TDS 680C, triggered from the picosecond pump laser. All experimental data for τ_{T10} are presented in Table 1. It is seen that, for most of the molecules in air-saturated solutions, τ_{T10} values are close and vary from 200 to 300 ns.

It is well-known that atmospheric oxygen is an effective quencher of the triplet state,[35] which will reduce the lifetime of the triplet state. Therefore, we performed triplet state lifetime measurements for several sulfur-containing squaraines in two solvents of different polarity, toluene and ACN, before and after oxygen removal using the procedure described in section.2.2.1. Due to the longer lifetime of the triplet state, it is reasonable to expect a larger effect of removing oxygen on τ_{T10} than on τ_S. A comparison of decay kinetics for air-saturated and nitrogen-purged toluene and ACN solutions for SD−SO 7517 is shown in Figure 6.

As seen, SD−S 7517 in both air-saturated solutions shows a single-exponential decay with τ_{T10} = 0.2−0.3 μs. As expected, oxygen removal leads to an increase of the triplet state lifetime, however, in different ways depending on solvent polarity. In low polar toluene solution, the single-exponential decay kinetics is changed to double-exponential decay with lifetimes of 0.9 and 4.2 μs. In polar ACN solution, triplet state decay kinetics remain single-exponential with τ_{T10} = 0.6 μs. The double-exponential decay of triplet state lifetime was also observed for all sulfur-containing squaraines in toluene after oxygen removal (as shown in Table 1), and can be explained by changing the order of the two low-lying triplet states of different orbital configuration (nπ* and ππ* nature) in nonpolar solvent. A similar effect was previously observed for aromatic carbonyl compounds.[50] On the basis of the explanation of ref 50, we can assume that the double-exponential kinetics in toluene corresponds to decay from the mixed nπ* and ππ* triplet states, while highly polar ACN, raising the energy of the ππ* triplet state with respect to the nπ* triplet state, shows no discernible long-lived component.

2.2.4. Two-Photon Absorption Measurements. 2PA spectra, measured by the femtosecond system, are obtained by two well-established methods: two-photon absorption induced fluorescence (2PF) and *Z*-scan techniques.[33,51] The 2PF represents an indirect way to measure the 2PA cross sections by comparing the integrated fluorescence signal from the investigated sample to a reference compound (with known 2PA

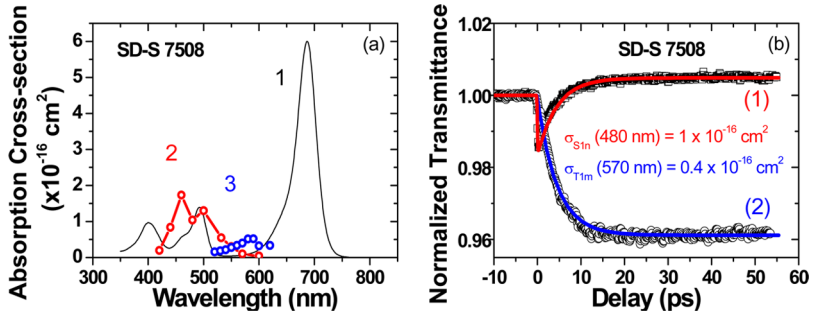

Figure 5. Linear absorption (1), S−S (2), and T−T (3) ESA absorption spectra (a) and decay kinetics (b) at 480 nm (pump fluence 0.5 mJ/cm^2, $\sigma_{S01} = 90\times 10^{-18}$ cm^2, $\sigma_{S1n} = 1 \times 10^{-16}$ cm^2, τ_S = 4.5 ps) (1) and 570 nm (pump fluence 0.5 mJ/cm^2, $\sigma_{S01} = 6.5\times 10^{-18}$ cm^2, $\sigma_{T1n} = 0.5 \times 10^{-16}$ cm^2, τ_S = 4.5 ps) (2) for SD−S 7508 in toluene.

dx.doi.org/10.1021/jp400276g | J. Phys. Chem. A 2013, 117, 2333−2346

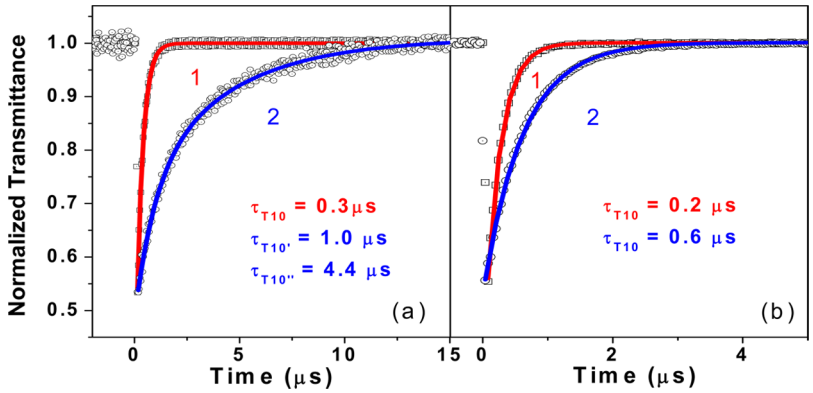

Figure 6. Triplet lifetime measurements for SD−S 7517 in (a) toluene and in (b) ACN. Shorter decays (1) correspond to air-saturated solutions, while longer decays (2) correspond to solutions with oxygen removed.

cross section) measured under identical conditions. It can thus be applied to the molecules with relatively large fluorescence quantum yields. The *Z*-scan, representing a direct way to measure the 2PA cross sections without the use of reference samples, may be applied to any compound, including nonfluorescent ones. In our previous paper,[15] we showed the similarity of 2PA spectra for oxygen-containing SD−O 2405 and its sulfur-substituted analogue SD−S 7508. Here we present the 2PA spectra for another pair of squaraine dyes SD−O 2053 and SD−SO 7517. Figure 7 shows 2PA spectra of these

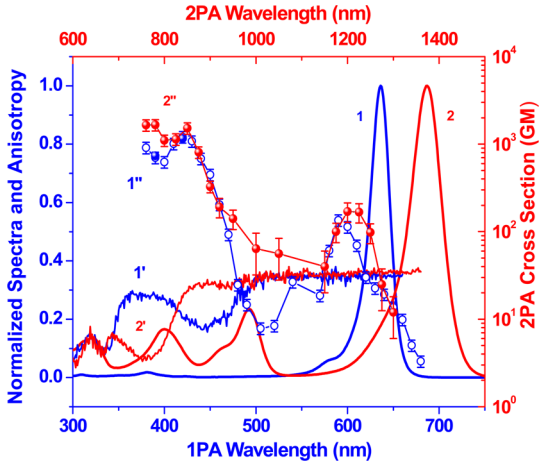

Figure 7. Normalized one-photon absorption (1, 2), excitation anisotropy (1′, 2′), and two-photon absorption spectra (1″, 2″) for SD−O 2053 (1, 1′, 1″) and SD−S 7517 (2, 2′, 2″). The two-photon excitation wavelengths and absorption cross sections are shown on the top and right axes, correspondingly. 2PA data shown by solid red circles for SD−S 7517 and solid blue circles for SD−O 2053 are obtained by open-aperture *Z*-scans. 2PA data shown by blue open circles for SD−O 2053 correspond to 2PF measurements. All spectra are measured in ACN, except excitation anisotropy in pTHF.

dyes in toluene solution along with their linear absorption and fluorescence excitation anisotropy spectra. Owing to its large Φ_F, the 2PA spectrum of SD−O 2053 in toluene was measured by 2PF; however, open apertures *Z*-scans at a few wavelengths were also performed to verify the δ_{2PA} values. The 2PA spectrum of SD−SO 7517 was measured with the open aperture *Z*-scan in a 1 mm flow cell to avoid photochemical damaging of this dye under strong laser irradiation. The flow rate, controlled by a tube pump (Masterflex), was set at ∼350 mL/min, which is fast enough to avoid multishot excitation of dye molecules. Note that, since 2PA is an instantaneous process, the flowing setup does not affect the 2PA signal.

It is seen from Figure 7 that both squaraine dyes exhibit similar 2PA spectra. The first 2PA bands are located at the vibrational shoulders of their $S_0 \rightarrow S_1$ transitions with similar $\delta_{2PA} \approx 200$ GM. Note that the "vibronic coupling" band for SD−SO 7517 is slightly red-shifted with respect to SD−O 2053, due to the red-shift of linear absorption peak. The positions of the second 2PA bands with $\delta_{2PA}^{max} = 1200$ GM at 840 nm coincide for both dyes. The third 2PA peaks cannot be resolved due to the presence of the linear absorption edges. The largest $\delta_{2PA} = 1660$ GM (at 760 nm) is observed for SD−SO 7517. This enhancement, as compared to SD−O 2053, can be attributed to the red-shift of the linear absorption peak for SD−SO 7517, leading to a smaller detuning energy and thus to intermediate state resonance enhancement.[52] On the basis of the previous data[15] and results of the current 2PA measurements, we can conclude that sulfur substitution in squaraine dyes does not significantly affect the energy structure of the singlet $\pi\pi^*$ states.

3. QUANTUM-CHEMICAL ANALYSIS

The electronic structure of the excited states were predicted with the Gaussian 2009 suite of programs.[53] The hybrid exchange-correlation density functional B3LYP[54] was used in combination with 6-31G* basis set.[55] The polarizable continuum model (PCM) in its solvation model density parametrization[56] was used to simulate the solvent effects (ethanol was chosen as the model solvent for PDs and toluene for SDs). Time-dependent density functional theory (TD-DFT)[57] was used to investigate the electronic structure of the three lowest singlet (S_i) and triplet (T_i) excited states. The excitation energies for these states, along with their dominant configurations, are reported in Table 2. Excitation energies for cyanine dyes are known to present a challenge for the TD-DFT method.[58] The physical reasons for this inaccuracy and a remedy to improve the excitation energy predictions was proposed recently.[59] In short, the electronic excitation in cyanine chain results in charge transfer between even and odd atoms of the chain. The TD-DFT method in the commonly used adiabatic approximation is evaluating the excited state energy in the potential generated by the ground state. This approximation works well when the electron density does not change much upon the excitation but results in larger than usual errors in cases like cyanine dyes. The improvement in

dx.doi.org/10.1021/jp400276g | J. Phys. Chem. A 2013, 117, 2333−2346

Table 2. Excitation Energies (E_{TD}, eV), Leading Singlet and Triplet Configurations, and Oscillator Strengths (Osc.) Predicted with TD-B3LYP/6-31G*/PCM, Singlet Excitation Energies Predicted with FD-B3LYP/6-31G*/PCM (E_{FD}, eV), and SOC Matrix Elements between Dominant Configurations of Each Triplet and the Lowest Singlet S_1, Calculated at the Planar Optimized S_1 Geometry, and Out-of-Plane Distorted S_1 Geometry

	E_{TD} (eV)	E_{FD} (eV)	leading singlet configuration	Osc.		E_{TD} (eV)	E_{FD} (eV)	leading triplet configuration	SOC in planar S_1 (cm^{-1})	SOC in distorted S_1 (cm^{-1})
							PD 1852			
S_1	2.18	1.84	HOMO → LUMO	2.61	T_1	1.30	1.24	HOMO → LUMO	0.00	0.00
S_2	2.93	3.08	HOMO-1 → LUMO	0.05	T_2	2.42	2.34	HOMO-1 → LUMO	0.20	22.1
S_3	3.15	3.01	HOMO-2 → LUMO	0.65	T_3	2.82	2.84	HOMO-2 → LUMO	0.00	0.00
							PD 2929			
S_1	2.33	1.91	HOMO → LUMO	2.92	T_1	1.34	1.39	HOMO → LUMO	0.00	0.02
S_2	3.33	3.03	HOMO-2 → LUMO	0.01	T_2	2.45	2.61	HOMO-1 → LUMO	0.04	0.38
S_3	3.71	3.76	HOMO-1 → LUMO	0.04	T_3	3.13	3.27	HOMO-2 → LUMO	0.00	0.00
							SD−O 2405			
S_1	2.10	1.77	HOMO → LUMO	3.13	T_1	1.01	1.21	HOMO → LUMO	0.00	0.15
S_2	2.15	3.38	HOMO-2 → LUMO	0.00	T_2	2.03	2.33	HOMO-1 → LUMO	0.00	5.10
S_3	3.12	3.35	HOMO-1 → LUMO	0.00	T_3	2.32	2.50	HOMO-2 → LUMO	0.00	0.00
							SD−S 7508			
S_1	1.72	1.76	HOMO-1 → LUMO	0.00	T_1	1.17	1.29	HOMO → LUMO	0.00	2.03
S_2	1.92	2.11	HOMO → LUMO	1.35	T_2	1.68	1.96	HOMO → LUMO+1	0.00	0.27
S_3	2.15	2.65	HOMO-2 → LUMO	0.00	T_3	2.02	2.13	HOMO-4 → LUMO	1.32	1.33

excitation energy can be achieved, however, when the relaxed density of the excited state obtained with the standard TD-DFT method is used to generate the potential instead of the ground state density. This can be practically accomplished when the static DFT is used on the excited Slater determinant built on the natural orbitals of the excited state, but the orbital optimization is not performed (this is known as frozen density approximation, FD-DFT). The excitation energies in the frozen density approximation, including sum rule spin-contamination correction, are reported as FD-DFT in Table 2. The ground states S_0 and the lowest singlet excited states S_1 were optimized with B3LYP/6-31G*/PCM and TDA-B3LYP/6-31G*/PCM, respectively, under the assumption of molecular planarity (point group C_{2v} for PD 1852 and PD 2929; point group C_{2h} for SD 2408 and SD 7508). In all S_0 and S_1 states for all four dyes, the vibrational analysis revealed two imaginary normal modes, corresponding to out-of-plane vibrational motions (belonging to irreducible representations A_2 and B_1 in the C_{2v} point group; A_u and B_g in the C_{2h} point group). The zero point vibrational energy test[60] was used to inspect whether this apparent nonplanarity is physically meaningful. A small step along the imaginary normal mode followed by the new optimization procedure lowered the total energy by less than 0.01 kcal/mol, while the zero point vibrational energy test increased the total energy by over 0.2 kcal/mol in all cases. Therefore, we conclude that their time-averaged dynamic structures (or the largest probabilities of the nuclear densities in quantum terms) for all these molecules in both S_0 and S_1 states are planar.

SOC matrix elements between the first excited singlet and the few lowest triplet states were calculated using the graphical unitary group approach capability in the GAMESS-US computer program (version 11, Aug 2011).[61] The one-electron approximation to the microscopic Breit−Pauli spin−orbit operator and effective nuclear charges were used.[62] The states for the SOC evaluations were constructed in the basis of single excitations in Kohn−Sham orbitals, with the active space including five HOMOs (HOMO-4, HOMO-3, HOMO-2, HOMO-1, HOMO) and two LUMOs (LUMO and LUMO +1).

It is well established that vibronic interactions can substantially increase the ISC rates, making El-Sayed forbidden transitions nearly as probable as El-Sayed allowed ones.[63] For instance, it is shown that in porphyrines vibronic spin−orbit terms, resulting from a sharp rise of the SOC components along the out-of-plane vibrational coordinates, can increase the ISC rate by 2 orders of magnitude.[64] Here we employ a similar method to investigate non-Franck−Condon effects on SOC matrix elements. For this purpose, the planar optimized geometry of the lowest singlet state S_1 was distorted out-of-plane along one of the normal modes. This normal mode was selected as the mode with the largest amplitude of the heaviest atom in the investigated molecule (Se, I, O, and S, respectively). The amplitude of this out-of-plane distortion was selected so that the total molecular energy is increased by ca. 0.6 kcal/mol (kT value at room temperature). The excitation energies and SOC components, obtained in the planar and distorted geometries, are presented in Table 2.

3.1. Quantum Chemical Analysis of PDs with "Heavy" Atoms. First, we analyze our experimental results obtained for the series of PDs with the "heavy"-atom substitutions: PDs 2929, 1852, 4216, and 2972. From our measurements, it follows that Φ_T for Br-substituted PD 2929 is the smallest, not exceeding 0.05. For both Se-substituted PDs 1852 and 2972, Φ_T are similar, 0.10 ± 0.05, indicating that additional incorporation of Br atoms into the chain in PD 2972 cannot increase Φ_T and the main effect is connected with "heavy" Se substitutions. Small values of Φ_T indicate that the fluorescence and internal conversion via singlet states are still dominating the deactivation pathways for PDs. These results have been explained by our quantum-chemical calculations, showing that both PD 1852 and PD 2929 have an intense lowest $S_0 \rightarrow S_1$ transition of $\pi-\pi^*$ nature involving HOMO and LUMO orbitals. As shown in Table 2 for PD 1852, only two triplets (T_1 and T_2) are found to be thermally accessible for ISC deactivation pathways (that is, below S_1 in energy as T_1, or within a few C−C vibrational quanta above it as T_2). The

dx.doi.org/10.1021/jp400276g | J. Phys. Chem. A 2013, 117, 2333−2346

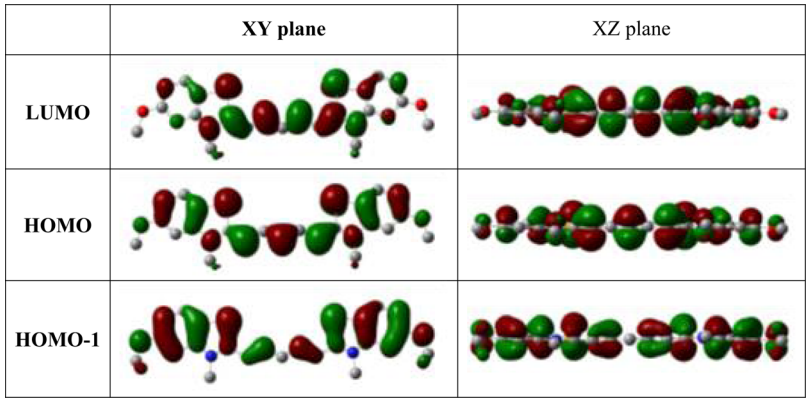

Figure 8. Isosurfaces of the essential Kohn–Sham orbitals in in *XY* and *XZ* planes for PD 1852.

essential orbitals involved in these transitions (HOMO → LUMO and HOMO-1 → LUMO) are shown in Figure 8. All triplet states for PD 1852 are of $\pi\pi^*$ nature. Therefore, ISC processes between the singlet (S_1) and triplet (T_1 and T_2) states of $\pi\pi^*$ nature are forbidden by El-Sayed rules.[29] The calculated SOC components are indeed small at the planar S_1 geometry. The largest T_2 SOC component is 0.2 cm^{-1}. Out-of-plane distortion, however, results in $\pi-\sigma^*$ mixing and a large (2 orders of magnitude) increase in the SOC component for T_2 in PD 1852. This state, however, is too high above S_1 (0.5 eV or 12 kcal/mol) to result in a large ISC rate. In PD 2929, this effect is much less pronounced, as HOMO-1 has a node in the center of the molecule at the position of the Br atom (unlike peripheral Se atoms in PD 1852), and ISC cannot efficiently compete with internal channels of relaxation, resulting in negligible triplet quantum yield. Negligibly small SOC elements are found for PD 4216 for all lower-lying triplets. Therefore, we may conclude that 10% triplet quantum yields for Se-substituted PD 1852 and PD 2972 are connected with non-Franck–Condon vibronic enhancement of the El-Sayed forbidden ISC channel.

3.2. Quantum Chemical Analysis of SDs. Now we analyze our experimental results for a series of oxygen- and sulfur-substituted squaraines. The main difference in the ISC rates between PDs and SDs arises from the nature of their first excited states. As one can see from Figure 9, HOMO-1 and HOMO-2 in SD 7508 are of n-type, the same as HOMO-2 in SD 2405 (not shown). These orbitals consist mostly of the *n*-lone pairs of S (or O) atoms and give rise to the low-lying $n\pi^*$ excited states (S_1, S_3, for SD 7508 and S_2 for SD 2405). However, not all El-Sayed allowed transitions have large SOC components according to our calculations; see Table 2. The noteworthy one is the S_1 ($n\pi^*$) → T_3 ($\pi\pi^*$) transition in SD 7508, probably thermally accessible, with a SOC component of 1.32 cm^{-1}, the largest among all planar S_1 geometries considered here. The vibronic coupling does not enhance this channel appreciably; however, it opens an additional El-Sayed allowed channel S_1 ($n\pi^*$) → T_1 ($\pi\pi^*$) with a SOC component of 2.03 cm^{-1}, favorable due to the small energy splitting between the singlet and triplet states. Calculations show that all squaraine molecules consist of two perpendicular conjugated chromophores: one placed in the horizontal plane between two nitrogen atoms (N–N chromophore), and the second placed in the vertical plane between two sulfur (S–S chromophore) or oxygen (O–O chromophore) atoms, as shown in Figure 9 for SD–S 7508. The main distinguishing feature of the vertical chromophore is the existence of unshared electron pairs

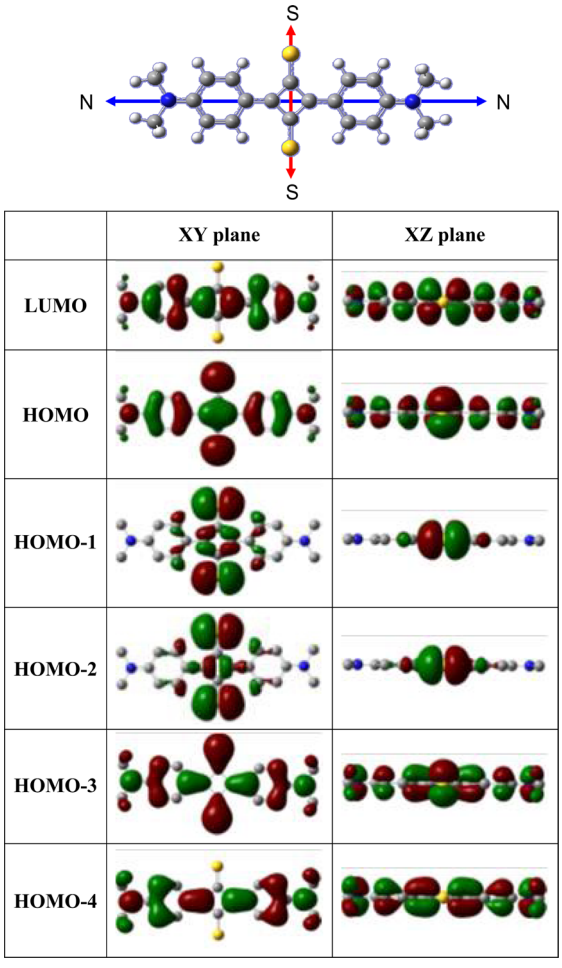

Figure 9. Molecular schematic of SD–S 7508 showing two perpendicular chromophores, one between nitrogen atoms (blue) and the second between sulfur atoms (yellow). The table presents isosurfaces of Kohn–Sham orbitals in *XY* and *XZ* planes for SD–S 7508.

producing states of $n\pi^*$ nature. On the basis of the origin of the charge distribution within the molecule, four types of MOs are responsible for the lowest electronic transitions, as shown in Figure 9 for SD–S 7508. The first type, presented by HOMO, and HOMO-3, corresponds to the totally delocalized π-orbitals with the charge spreading to both perpendicular π-conjugated chromophores. The second type of orbitals, presented by HOMO-1 and HOMO-2, corresponds to n-type and involve

dx.doi.org/10.1021/jp400276g | J. Phys. Chem. A 2013, 117, 2333–2346

the charge localized at the sulfur atoms, as clearly seen in the *XZ* plane of Figure 9. The third and fourth types are π-MOs involving the charge distributed only within the horizontal (N−N) or vertical (S−S) chromophores. Examples are LUMO and LUMO+1, respectively. Calculations show that the electronic transition lowest in energy corresponds to HOMO-1 → LUMO and is of the n−π^* nature. This n−π^* transition, being of very small oscillator strength, is covered by the next intense transition of π−π^* nature, related to HOMO → LUMO, which we typically consider as the main $S_0 \rightarrow S_1$ transition. Calculations suggest that replacing the oxygen atoms in a squaraine ring (SD−O 2405 structure) with sulfur atoms (SD−S 7508 structure) results in an inversion of the lowest π−π^* transition in SD−O 2405 by an n−π^* transition in SD−S 7508, so that two ISC channels become available: S_1 (nπ^*) → T_3 ($\pi\pi^*$), thermally accessible in the planar excited state geometry and an enhanced S_1 (nπ^*) → T_1 ($\pi\pi^*$) transition in the distorted S_1 geometry.

4. CONCLUSION

Linear and nonlinear spectroscopic properties of a series of polymethine dyes with Br- and Se-atom substitution, and a series of new squaraine molecules, where one or two oxygen atoms in a squaraine bridge are replaced with sulfur atoms, were investigated both experimentally and theoretically with the goal of understanding the efficiency of ISC processes in polymethine-like molecules. Using the double pump−probe technique, we determined that "heavy" Br- and Se-atom substitution in PDs does not significantly enhance singlet−triplet mixing probabilities. These dyes are characterized by small triplet quantum yields ($\Phi_T \leq 10\%$), indicating that the internal conversion via singlet states is a dominating deactivation pathway. Our results have been explained by quantum-chemical calculations at the TD-B3LYP/6-31G*/PCM level, showing that "heavy" Br and Se atoms do not significantly affect the charge distribution within the frontier orbitals, HOMO and LUMO, which are responsible for the main $S_0 \rightarrow S_1$ transitions for these molecular structures. Small, yet measurable, triplet quantum yields are explained by π−σ^* mixing in the out-of-plane distorted geometry of the S_1 state.

In contrast, the values of Φ_T and singlet oxygen generation for sulfur-containing SDs reach almost unity. We performed a detailed comparison of a series of sulfur-containing squaraines versus their oxygen-containing analogues. Quantum chemical calculations suggest that replacing the oxygen atoms in a squaraine ring by sulfur atoms leads to an inversion of the energy levels between the lowest π−π^* transition (occurring in SD−O molecules) and n−π^* transition (occurring in SD−S molecules), thus significantly reducing the singlet−triplet energy difference, and opening an additional ISC channel connected with non-Franck−Condon vibronic enhancement of the S_1 (nπ^*) → T_1 ($\pi\pi^*$) transition. Importantly, this inversion, affecting the ISC rate, does not lead to significant changes of the nonlinear optical properties of the molecules, such as ESA and 2PA.

In summary, we established a new approach to achieve polymethine-like molecules (sulfur-containing squaraines) having large triplet and singlet oxygen generation quantum yields (up to 100%), large two-photon absorption cross sections (up to 2000 GM), and large S−S and T−T absorption cross sections (up to 4×10^{-16} cm^2), potentially useful for applications in optical power regulation and photodynamic therapy.

AUTHOR INFORMATION

Corresponding Author

*E-mail: ewvs@creol.ucf.edu.

Notes

The authors declare no competing financial interest.

ACKNOWLEDGMENTS

We gratefully acknowledge support of the U.S. Army Research Laboratory and the U.S. Army Research Office (50372-CH-MUR) and the Israel Ministry of Defense (993/54250-01). We thank Lazaro A. Padilha for useful input.

REFERENCES

(1) Tyutyulkov, N. *Polymethine Dyes Structure and Properties*; Ohridski University Press: Sofia, St. Kliment, 1991.

(2) Fabian, J.; Nakazumi, H.; Matsuoka, M. Near-Infrared Absorbing Dyes. *Chem. Rev.* **1992**, *92*, 1197−1226.

(3) Spitler, M. T.; Ehret, A.; Kietzmann, R.; Willig, F. Electron Transfer Threshold for Spectral Sensitization of Silver Halides by Monomeric Cyanine Dyes. *J. Phys. Chem. B* **1997**, *101*, 2552−2557.

(4) Dempsey, G. T.; Bates, M.; Kowtoniuk, W. E.; Liu, D. R.; Tsien, R. Y.; Zhuang, X. Photoswitching Mechanism of Cyanine Dyes. *J. Am. Chem. Soc.* **2009**, *131*, 18192−18193.

(5) Christie, R. M. *Colour Chemistry*; The Royal Society of Chemistry: Cambridge, U.K., 2001.

(6) Mishra, A.; Behera, R. K.; Behera, P. K.; Mishra, B. K.; Behera, G. B. Cyanines during the 1990s: A Review. *Chem. Rev.* **2000**, *100*, 1973−2012.

(7) Fabian, J.; Nakazumi, H.; Matsuoka, M. Near-Infrared Absorbing Dyes. *Chem. Rev.* **1992**, *92*, 1197−1226.

(8) Negres, R. A.; Przhonska, O. V.; Hagan, D. J.; Van Stryland, E. W.; Bondar, M. V.; Slominsky, Y. L.; Kachkovski, A. D. The Nature of Excited-State Absorption in Polymethine and Squarylium Molecules. *IEEE J. Sel. Top. Quantum Electron.* **2001**, *7*, 849−863.

(9) Lepkowicz, R. S.; Przhonska, O. V.; Hales, J. M.; Fu, J.; Hagan, D. J.; Van Stryland, E. W.; Bondar, M. V.; Slominsky, Y. L.; Kachkovski, A. D. Nature of the Electronic Transitions in Thiacarbocyanines with a Long Polymethine Chain. *Chem. Phys.* **2004**, *305*, 259−270.

(10) Lim, J. H.; Przhonska, O. V.; Khodja, S.; Yang, S.; Ross, T. S.; Hagan, D. J.; Van Stryland, E. W.; Bondar, M. V.; Slominsky, Y. L. Polymethine and Squarylium Molecules with Large Excited-State Absorption. *Chem. Phys.* **1999**, *245*, 79−97.

(11) Beverina, L.; Crippa, M.; Landenna, M.; Ruffo, R.; Salice, P.; Silvestri, F.; Versari, S.; Villa, A.; Ciaffoni, L.; Collini, E.; Ferrante, C.; Bradamante, S.; Mari, C. M.; Bozio, R.; Pagani, G. A. Assessment of Water-Soluble Π-Extended Squaraines as One- and Two-Photon Singlet Oxygen Photosensitizers: Design, Synthesis, and Characterization. *J. Am. Chem. Soc.* **2008**, *130*, 1894−1902.

(12) Santos, P. F.; Reis, L. V.; Duarte, I.; Serrano, J. P.; Almeida, P.; Oliveira, A. S.; Ferreira, L. F. V. Synthesis and Photochemical Evaluation of Iodinated Squarylium Cyanine Dyes. *Helv. Chim. Acta* **2005**, *88*, 1135−1143.

(13) Salice, P.; Arnbjerg, J.; Pedersen, B. W.; Toftegaard, R.; Beverina, L.; Pagani, G. A.; Ogilby, P. R. Photophysics of Squaraine Dyes: Role of Charge-Transfer in Singlet Oxygen Production and Removal. *J. Phys. Chem. A* **2010**, *114*, 2518−2525.

(14) Ogava, K.; Kobuke, Y. Recent Advances in Two-Photon Photodynamic Therapy. *Anti-Cancer Agents Med. Chem.* **2008**, *8*, 269−279.

(15) Webster, S.; Peceli, D.; Hu, H.; Padilha, L. A.; Przhonska, O. V.; Masunov, A. E.; Gerasov, A. O.; Kachkovski, A. D.; Slominsky, Y. L.; Tolmachev, A. I.; et al. Near-Unity Quantum Yields for Intersystem Crossing and Singlet Oxygen Generation in Polymethine-Like Molecules: Design and Experimental Realization. *J. Phys. Chem. Lett.* **2010**, *1*, 2354−2360.

(16) Brown, S. Photodynamic Therapy: Two Photons Are Better Than One. *Nat Photonics* **2008**, *2*, 394−395.

(17) Starkey, J. R.; Rebane, A. K.; Drobizhev, M. A.; Meng, F.; Gong, A.; Elliott, A.; McInnerney, K.; Spangler, C. W. New Two-Photon Activated Photodynamic Therapy Sensitizers Induce Xenograft Tumor Regressions after Near-Ir Laser Treatment through the Body of the Host Mouse. *Clin. Cancer Res.* **2008**, *14*, 6564−6573.
(18) Frederiksen, P. K.; Jørgensen, M.; Ogilby, P. R. Two-Photon Photosensitized Production of Singlet Oxygen. *J. Am. Chem. Soc.* **2001**, *123*, 1215−1221.
(19) Dou, K.; Xiaodong, S.; Xiaojun, W.; Parkhill, R.; Yin, G.; Knobbe, E. T. Optical Limiting and Nonlinear Absorption of Excited States in Metalloporphyrin-Doped Sol Gels. *IEEE J. Quantum Electron.* **1999**, *35*, 1004−1014.
(20) Xia, T.; Hagan, D. J.; Dogariu, A.; Said, A. A.; Van Stryland, E. W. Optimization of Optical Limiting Devices Based on Excited-State Absorption. *Appl. Opt.* **1997**, *36*, 4110−4122.
(21) Lepkowicz, R.; Kobyakov, A.; Hagan, D. J.; Van Stryland, E. W. Picosecond Optical Limiting in Reverse Saturable Absorbers: A Theoretical and Experimental Study. *J. Opt. Soc. Am. B* **2002**, *19*, 94−101.
(22) Song, Y.; Fang, G.; Wang, Y.; Liu, S.; Li, C.; Song, L.; Zhu, Y.; Hu, Q. Excited-State Absorption and Optical-Limiting Properties of Organometallic Fullerene–C_{60} Derivatives. *Appl. Phys. Lett.* **1999**, *74*, 332−334.
(23) Lawetz, V.; Orlandi, G.; Siebrand, W. Theory of Intersystem Crossing in Aromatic Hydrocarbons. *J. Chem. Phys.* **1972**, *56*, 4058−4072.
(24) Robinson, G. W.; Frosch, R. P. Electronic Excitation Transfer and Relaxation. *J. Chem. Phys.* **1963**, *38*, 1187−1203.
(25) Lower, S. K.; El-Sayed, M. A. The Triplet State and Molecular Electronic Processes in Organic Molecules. *Chem. Rev.* **1966**, *66*, 199−241.
(26) Solov'ev, K. N.; Borisevich, E. A. Intramolecular Heavy-Atom Effect in the Photophysics of Organic Molecules. *Phys.-Usp.* **2005**, *48*, 231−253.
(27) Schmidt, K.; Brovelli, S.; Coropceanu, V.; Beljonne, D.; Cornil, J.; Bazzini, C.; Caronna, T.; Tubino, R.; Meinardi, F.; Shuai, Z.; Brédas, J.-L. Intersystem Crossing Processes in Nonplanar Aromatic Heterocyclic Molecules. *J. Phys. Chem. A* **2007**, *111*, 10490−10499.
(28) Detty, M. R.; Merkel, P. B. Chalcogenapyrylium Dyes as Potential Photochemotherapeutic Agents. Solution Studies of Heavy Atom Effects on Triplet Yields, Quantum Efficiencies of Singlet Oxygen Generation, Rates of Reaction with Singlet Oxygen, and Emission Quantum Yields. *J. Am. Chem. Soc.* **1990**, *112*, 3845−3855.
(29) El-Sayed, M. A. Spin—Orbit Coupling and the Radiationless Processes in Nitrogen Heterocyclics. *J. Chem. Phys.* **1963**, *38*, 2834−2838.
(30) Englman, R.; Jortner, J. The Energy Gap Law for Radiationless Transitions in Large Molecules. *Mol. Phys.* **1970**, *18*, 145−164.
(31) Swatton, S. N. R.; Welford, K. R.; Hollins, R. C.; Sambles, J. R. A Time Resolved Double Pump-Probe Experimental Technique to Characterize Excited-State Parameters of Organic Dyes. *Appl. Phys. Lett.* **1997**, *71*, 10−12.
(32) Peceli, D.; Webster, S.; Fishman, D. A.; Cirloganu, C. M.; Hu, H.; Przhonska, O. V.; Kurdyukov, V. V.; Slominsky, Y. L.; Tolmachev, A. I.; Kachkovski, A. D.; et al. Optimization of the Double Pump−Probe Technique: Decoupling the Triplet Yield and Cross Section. *J. Phys. Chem. A* **2012**, *116*, 4833−4841.
(33) Sheik-Bahae, M.; Said, A. A.; Wei, T. H.; Hagan, D. J.; Van Stryland, E. W. Sensitive Measurement of Optical Nonlinearities Using a Single Beam. *IEEE J. Quantum Electron.* **1990**, *26*, 760−769.
(34) Magde, D.; Brannon, J. H.; Cremers, T. L.; Olmsted, J. Absolute Luminescence Yield of Cresyl Violet. A Standard for the Red. *J. Phys. Chem.* **1979**, *83*, 696−699.
(35) Lakowicz, J. R. *Principles of Fluorescence Microscopy*; Kluwer Academic: New York, 1999.
(36) Przhonska, O. V.; Webster, S.; Padilha, L. A.; Hu, H.; Kachkovski, A. D.; Hagan, D. J.; Van Stryland, E. W. Two-Photon Absorption in Near-Ir Conjugated Molecules: Design Strategy and Structure−Property Relations. *Springer Ser. Fluoresc.* **2010**, *8*, 105−148.
(37) Wilkinson, F.; Helman, W. P.; Ross, A. B. Quantum Yields for the Photosensitized Formation of the Lowest Electronically Excited Singlet State of Molecular Oxygen in Solution. *J. Phys. Chem. Ref. Data* **1993**, *22*, 113−262.
(38) McClure, D. S. Triplet-Singlet Transitions in Organic Molecules. Lifetime Measurements of the Triplet State. *J. Chem. Phys.* **1949**, *17*, 905−913.
(39) Guo, S.; Wu, W.; Guo, H.; Zhao, J. Room-Temperature Long-Lived Triplet Excited States of Naphthalenediimides and Their Applications as Organic Triplet Photosensitizers for Photooxidation and Triplet−Triplet Annihilation Upconversions. *J. Org. Chem.* **2012**, *77*, 3933−3943.
(40) Kodama, N.; Sasaki, N.; Yamaga, M.; Masui, Y. Long-Lasting Phosphorescence of Eu2+ in Melilite. *J. Lumin.* **2001**, *94*−*95*, 19−22.
(41) Perry, J. W.; Mansour, K.; Lee, I.-Y. S.; Wu, X.-L.; Bedworth, P. V.; Chen, C.-T.; Ng, D.; Marder, S. R.; Miles, P.; Wada, T.; Tian, M.; Sasabe, H. Organic Optical Limiter with a Strong Nonlinear Absorptive Response. *Science* **1996**, *273*, 1533−1536.
(42) van Amerongen, H.; van Grondelle, R. In *Methods Enzymol.*; Kenneth, S., Ed.; Academic Press: 1995; Vol. *246*, pp 201−226.
(43) Maciejewski, A.; Naskrecki, R.; Lorenc, M.; Ziolek, M.; Karolczak, J.; Kubicki, J.; Matysiak, M.; Szymanski, M. Transient Absorption Experimental Set-up with Femtosecond Time Resolution. Femto- and Picosecond Study of Dcm Molecule in Cyclohexane and Methanol Solution. *J. Mol. Struct.* **2000**, *555*, 1−13.
(44) Lessing, H. E.; Von Jena, A. Separation of Rotational Diffusion and Level Kinetics in Transient Absorption Spectroscopy. *Chem. Phys. Lett.* **1976**, *42*, 213−217.
(45) van Veenendaal, M.; Chang, J.; Fedro, A. J. Model of Ultrafast Intersystem Crossing in Photoexcited Transition-Metal Organic Compounds. *Phys. Rev. Lett.* **2010**, *104*, 067401-1−067401-2.
(46) Hedley, G. J.; Ruseckas, A.; Samuel, I. D. W. Ultrafast Intersystem Crossing in a Red Phosphorescent Iridium Complex. *J. Phys. Chem. A* **2008**, *113*, 2−4.
(47) Ramakrishna, G.; Goodson, T.; Rogers-Haley, J. E.; Cooper, T. M.; McLean, D. G.; Urbas, A. Ultrafast Intersystem Crossing: Excited State Dynamics of Platinum Acetylide Complexes. *J. Phys. Chem. C* **2008**, *113*, 1060−1066.
(48) Padilha, L. A.; Webster, S.; Hu, H.; Przhonska, O. V.; Hagan, D. J.; Van Stryland, E. W.; Bondar, M. V.; Davydenko, I. G.; Slominsky, Y. L.; Kachkovski, A. D. Excited State Absorption and Decay Kinetics of near Ir Polymethine Dyes. *Chem. Phys.* **2008**, *352*, 97−105.
(49) Padilha, L. A.; Webster, S.; Przhonska, O. V.; Hu, H.; Peceli, D.; Rosch, J. L.; Bondar, M. V.; Gerasov, A. O.; Kovtun, Y. P.; Shandura, M. P.; et al. Nonlinear Absorption in a Series of Donor-Π-Acceptor Cyanines with Different Conjugation Lengths. *J. Mater. Chem.* **2009**, *19*, 7503−7513.
(50) Rauh, R. D.; Leermakers, P. A. Solvent Effects Upon the Phosphorescence Lifetimes and Photoreactivity of Butyrophenone. *J. Am. Chem. Soc.* **1968**, *90*, 2246−2249.
(51) Xu, C.; Webb, W. W. Measurement of Two-Photon Excitation Cross Sections of Molecular Fluorophores with Data from 690 to 1050 Nm. *J. Opt. Soc. Am. B* **1996**, *13*, 481−491.
(52) Hales, J. M.; Hagan, D. J.; Stryland, E. W. V.; Schafer, K. J.; Morales, A. R.; Belfield, K. D.; Pacher, P.; Kwon, O.; Zojer, E.; Bredas, J. L. Resonant Enhancement of Two-Photon Absorption in Substituted Fluorene Molecules. *J. Chem. Phys.* **2004**, *121*, 3152−3160.
(53) Frisch, M. J.; Trucks, G. W.; Schlegel, H. B.; Scuseria, G. E.; Robb, M. A.; Cheeseman, J. R.; Scalmani, G.; Barone, V.; Mennucci, B.; Petersson, G. A.; et al.; *Gaussian 09*; Gaussian, Inc.: Wallingford, CT, 2009.
(54) Becke, A. D. Density-Functional Thermochemistry. Iii. The Role of Exact Exchange. *J. Chem. Phys.* **1993**, *98*, 5648−5652.
(55) Rassolov, V. A.; Pople, J. A.; Ratner, M. A.; Windus, T. L. 6-31g[Sup *] Basis Set for Atoms K through Zn. *J. Chem. Phys.* **1998**, *109*, 1223−1229.
(56) Marenich, A. V.; Cramer, C. J.; Truhlar, D. G. Universal Solvation Model Based on Solute Electron Density and on a Continuum Model of the Solvent Defined by the Bulk Dielectric

Constant and Atomic Surface Tensions. *J. Phys. Chem. B* **2009**, *113*, 6378−6396.
(57) Casida, M. E.; Jamorski, C.; Casida, K. C.; Salahub, D. R. Molecular Excitation Energies to High-Lying Bound States from Time-Dependent Density-Functional Response Theory: Characterization and Correction of the Time-Dependent Local Density Approximation Ionization Threshold. *J. Chem. Phys.* **1998**, *108*, 4439−4449.
(58) Fabian, J. Tddft-Calculations of Vis/Nir Absorbing Compounds. *Dyes Pigm.* **2010**, *84*, 36−53.
(59) Masunov, A. E. Theoretical Spectroscopy of Carbocyanine Dyes Made Accurate by Frozen Density Correction to Excitation Energies Obtained by Td-Dft. *Int. J. Quantum Chem.* **2010**, *110*, 3095−3100.
(60) Masunov, A.; Dannenberg, J. J. Theoretical Study of Urea. I. Monomers and Dimers. *J. Phys. Chem. A* **1999**, *103*, 178−184.
(61) Schmidt, M. W.; Baldridge, K. K.; Boatz, J. A.; Elbert, S. T.; Gordon, M. S.; Jensen, J. H.; Koseki, S.; Matsunaga, N.; Nguyen, K. A.; Su, S.; Windus, T. L.; Dupuis, M.; Montgomery, J. A. General Atomic and Molecular Electronic Structure System. *J. Comput. Chem.* **1993**, *14*, 1347−1363.
(62) Fedorov, D. G.; Koseki, S.; Schmidt, M. W.; Gordon, M. S. Spin-Orbit Coupling in Molecules: Chemistry beyond the Adiabatic Approximation. *Int. Rev. Phys. Chem.* **2003**, *22*, 551−592.
(63) Marian, C. M. Spin−Orbit Coupling and Intersystem Crossing in Molecules. *Wiley Interdiscip. Rev.: Comput. Mol. Sci.* **2012**, *2*, 187−203.
(64) Perun, S.; Tatchen, J.; Marian, C. M. Singlet and Triplet Excited States and Intersystem Crossing in Free-Base Porphyrin: Tddft and Dft/Mrci Study. *ChemPhysChem* **2008**, *9*, 282−292.